TÜBİTAK

Turkish Journal of Chemistry

http://journals.tubitak.gov.tr/chem/

Research Article

Turk J Chem
(2013) 37: 182 – 194
© TÜBİTAK
doi:10.3906/kim-1202-65

Synthesis and characterization of thermally stable camphor-based polyimide–clay nanocomposites

Murat YİĞİT,[1] Turgay SEÇKİN,[2,*] Beyhan YİĞİT,[1] Süleyman KÖYTEPE[2]

[1]Chemistry Department, Faculty of Arts and Science, Adıyaman University, Adıyaman, Turkey

[2]Chemistry Department, Faculty of Arts and Science, İnönü University, 44280, Malatya, Turkey

Received: 28.02.2012 • **Accepted:** 04.12.2012 • **Published Online:** 17.04.2013 • **Printed:** 13.05.2013

Abstract: A new monomer was prepared from (1R,3S)-(+)-camphoric acid. Novel polyimide and polyimide–clay hybrid composites were developed from one-pot condensation reactions of this monomer and pyromellitic dianhyride. Polyimide-montmorillonite nanocomposites were prepared from solution of polyimide and with different weight percentages (1, 5, 10 wt %) of organo-modified montmorillonite (OM-MMT) using *N*-methyl-2-pyrrolidone (NMP) as aprotic solvent. The reactive organoclay was formed by using hexadecylpyridinium chloride as a swelling agent for silicate layers of montmorillonite. The polyimide–clay composites films (PI–MMT) were characterized by Fourier transform infrared spectroscopy, scanning electron microscopy (SEM), and X-ray diffraction (XRD). All composites were subjected to differential scanning calorimetry measurements for the purpose of examining Tg from all compositions. The clay content significantly influenced the thermal behavior of the polymeric films, such as glass transition and decomposition temperatures of polyimide–clay composites. The glass transition temperatures of the composites were higher than that of the original polyimide. Their thermal decomposition temperatures (Td = temperature at 5% mass loss) were measured via thermogravimetric analysis and showed that the introduction of clay into polymer backbones increased thermal stability. SEM, XRD, and the other conventional techniques were used for structural characterization. Dispersion of the modified clay in the polyimide matrix resulted in nanostructured material containing intercalated polymer between the silicate layers. The morphology and properties of PI nanocomposites greatly depend on the functional groups of the organic modifiers, synthesis procedure, and structure of polyimide because of the chemical reactions and physical interactions involved.

Key words: Polyimide, nanocomposites, organoclay, clay dispersion

1. Introduction

Polymer composites are widely used in electronic and information products, consumer commodities, and the construction industry. In these polymer composites, inorganic materials are used to reinforce polymers with the idea of taking advantage of the high heat durability and the high mechanical strength of the inorganic materials and the ease of processing polymers.[1–5] The polymer matrices that have been widely used in nanocomposite design include poly(vinyl alcohol), styrene-butadiene rubber, epoxy resins, polyethylene, polyurethanes, polyamides, polyimides, etc.[5–10] Different types of nanofillers (including ceramic and metallic nanopowders, nano-clay, carbon nanotubes (CNTs), nano-SiO_2, etc.) have been used to reinforce the polymer matrix.[11–14] Clays have been extensively used in the polymer industry either as a reinforcing agent to improve the physicomechanical

*Correspondence: tseckin@inonu.edu.tr

properties of the final polymer or as a filler to reduce the amount of polymer used in the shaped structures, i.e. to act as a diluent for the polymer, thereby lowering the high financial cost of the polymer systems.[1] In general, a large amount of filler is necessary to improve the desired properties of the polymer. Clay minerals, and particularly smectites, seem to be suitable fillers for improving the different polymers' properties. It is observed that a small amount of well-dispersed clay mineral in the polymer matrix drastically improves its properties. However, studies on polymer/clay nanocomposites have been successfully extended to many other polymer systems.[15]

Polyimide (PI) composites have been proposed or are being used for numerous applications, ranging from sensors to advanced optoelectronic devices.[16–18] Understanding the impact of fillers on the composite's mechanical properties is critical to the success of all of these applications. Consequently, a large number of research groups are focused on developing a general framework for predicting or at least understanding how the chemistry and morphology of the polymer matrix synergize with the surface chemistry, the size, and the shape of a scale filler to define mechanical properties.[19–23]

Clay is a type of layered silicate. The most commonly used clay in the preparation of PI–clay nanocomposites is montmorillonite (MMT). It is about 100–218 nm in length and 1 nm in thickness. Montmorillonite is also called philo-silicate with 1 octahedral Al_2O_3 sheet between 2 tetrahedral SiO_2 sheets.[24] It can be intercalated or exfoliated in a polymer matrix to form the nanocomposite. The effects of clay type, clay content, and PI molecular structure on clay dispersion in thermoplastic PI nanocomposites have been studied. It has been found that MMT clays exchanged with long chain onium ions have good compatibility with polyimide. The extent of gallery expansion of modified MMT is mainly determined by the chain length of the gallery onium ions.[4] A good dispersion of layered silicate has been found to improve the properties of PI nanocomposites, such as mechanical properties, thermal stability, and gas permeability.[5–7] Good dispersion of clays in the PI matrix has been achieved through the modification of MMT with active organic modifiers.

This article reports on polyimide–clay nanocomposite (PI–MMT) materials, consisting of (1R,3S)-(+)-1,2,2-trimethyl-1,3-bis(p-dimethylamino benzyliden amino)-cyclopentane with different weight percentages (1, 5, 10 wt %) of clay, successfully prepared by solution dispersion. The as-synthesized PI–MMT nanocomposites were subsequently characterized by Fourier transform infrared (FT-IR) spectroscopy, X-ray diffraction (XRD), and scanning electron microscopy (SEM). These studies showed the homogeneous dispersion of clay in the polyimide matrix with an increase in the thermal steadiness of the composite films on clay loadings.

2. Experimental

2.1. Materials

All chemicals were purchased from Aldrich and used after purification. *N*-methyl-2-pyrrolidone (NMP) was distilled over CaH_2 under reduced pressure and stored over 4-Å molecular sieves. Reagent grade pyromellitic dianhydride (PMDA) that was sublimed at 250 °C under reduced pressure was used after crystallization from the appropriate solvents. The dianhydride was dried under vacuum at 120 °C prior to use. Natural montmorillonite clay from the Reşadiye region of Tokat, Turkey, was used in this work. The Na-montmorillonite was obtained by the methods of dispersion and sedimentation and various chemical treatments applied to natural clay.[25] Finally, it was washed with water until neutral pH was obtained. The material was dried in an oven at 353 K for 24 h. To make an organically modified montmorillonite for better dispersion of MMT in a polymer matrix, 2 g of purified MMT was completely dissolved in 100 mL of deionized water at 75 °C with vigorous stirring

for 24 h. The pyridinium catyonic solution, which was prepared by dissolving 0.67 g of hexadecylpyridinium chloride (HPC) in 50 mL of ethanol, was added to the dissolved Na-MMT solution, and mixed for a further 24 h at 75 °C. The organically treated MMT (O-MMT) was washed repeatedly with a fresh 2:1 mixture of deionized water and ethanol until no further AgCl formed with titration with 0.1 N $AgNO_3$. The product was then filtered and dried in a vacuum oven at 30 °C for 24 h. The composition and specific surface area of the treated clay were as follows: SiO_2 88%, Al_2O_3 5.2%, Fe_2O_3 2.7%, CaO 0.26%, MgO 0.17%, Na_2O 0.1%, K_2O 0.48%, MnO_2 0.08%; SBET = 112.3 m^2/g.

2.2. Measurements

FT-IR spectra were recorded as KBr pellets in the range 400–4000 cm^{-1} on an ATI UNICAM 1000 Fourier transform spectrometer. ^{1}H NMR and ^{13}C NMR spectra were recorded in $CDCl_3$ with tetramethylsilane as an internal reference using a Varian As 400 Merkur spectrometer operating at 400 MHz (1H) or 100 MHz (13C). The NMR studies were carried out in high-quality 5-mm NMR tubes. Signals are quoted in parts per million as δ downfield from tetramethylsilane (δ 0.00) as an internal standard. Coupling constants (J values) are given in hertz. NMR multiplicities are abbreviated as follows: s = singlet, d = doublet, t = triplet, m = multiplet signal. Elemental analyses were performed by the TÜBİTAK Microlab (Ankara, Turkey).

Differential scanning calorimetry (DSC) and thermogravimetric analysis (TGA) were performed at a heating rate of 10 °C min^{-1} in air atmosphere, with Shimadzu DSC-60 and TGA-50 thermal analyzers, respectively.

The samples were characterized by XRD for the crystal structure, average particle size, and the concentration of impurity compounds present. A Rigaku Rad B-Dmax II powder X-ray diffractometer was used for XRD patterns of these samples. The 2θ values were taken from 20° to 110° with a step size of 0.04° using Cu Kα radiation (λ value of 2.2897 Å). The dried samples were dusted onto plates with low background. A small quantity of 30($\pm$2) mg spread over a 5 cm^2 area was used to minimize errors in peak location and also reduce the broadening of peaks due to thickness of the sample. These data illustrate the crystal structure of the particles and provide the inter-planar space, d. The broadening of the peak was related to the average diameter (L) of the particle according to Scherrer's formula, i.e. $L = 0.9\lambda/\Delta \cos \theta$, where λ is X-ray wavelength, Δ is line broadening measured at half-height, and θ is the Bragg angle of the particles.

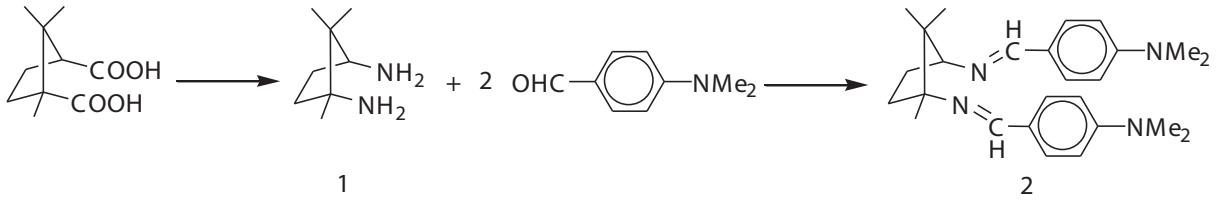
Chemical composition analysis by EDAX was performed with a Rönteck XFlash detector analyzer connected to a scanning electron microscope (SEM, Leo-Evo 40XVP). Incident electron beam energies from 3 to 30 keV were used. In all cases, the beam was at normal incidence to the sample surface and the measurement time was 100 s. All the EDAX spectra were corrected by using ZAF (atomic number, absorption, and fluorescence) correction, which takes into account the influence of the matrix material on the obtained spectra.

2.3. Synthesis of the monomer (1R,3S)-(+)-1,2,2-trimethyl-1,3-bis(p-dimethylamino benzyliden amino)-cyclopentane (2)

(1R,3S)-(+)-1,2,2-trimethyl-1,3-diaminocyclopentane (**1**) was prepared from (1R,3S)-(+)-camphoric acid according to the literature.[26]

(1R,3S)-(+)-1,2,2-trimethyl-1,3-bis(p-dimethylamino benzyliden amino)-cyclopentane (**2**) from **1** and p-dimethylaminobenzaldehyde was synthesized by nucleophilic addition reaction (Scheme 1). A mixture of toluene (50 mL), p-dimethylaminobenzaldehyde (3.28 g, 22 mmol), (1R,3S)-(+)-1,2,2-trimethyl-1,3-diaminocyclopentane

(**1**) (1.56 g, 11 mmol), and *p*-toluenesulfonic acid (0.01 g) was stirred under reflux for 4 h. After evaporation of the solvent, the crude product was recrystallized from toluene (20 mL)/hexane (5 mL) to give a yellow solid. Yield 2.81 g (63%), mp 196 °C, $\nu_{(C=N)} = 1556$ cm^{-1}, $[\alpha]_D^{20} = +110$ (c 0.4 in CH_2Cl_2).



1 2

Scheme 1. The synthetic route for the preparation of the monomers.

^{1}H NMR (δ, $CDCl_3$): a; 0.89 (s, 3H, CH_3), b; 0.93 (s, 3H, CH_3), c; 1.20 (s, 3H, CH_3), d and e; 1.73, 2.01 and 2.28 (m, 4H, CH_2CH_2), f; 3.49 (t, 1H, $J = 8.4$ Hz, CH), g; 3.00 (s, 12H, $N(CH_3)_2$), h and i; 6.70 and 7.65 (m, 8H, Ar-H), j; 8.15 (s, 2H, CH =N) (Figure 1). ^{13}C NMR (δ, $CDCl_3$): 18.91, 21.15 and 25.00 ($3CH_3$), 40.56 and 40.62 ($N(CH_3)_2$), 28.35, 34.56, 49.28 and 70.62 ($C_{cyclopentane}$), 111.94, 112.06, 125.43, 126.52, 129.28, 129.72, 152.09 and 155.74 ($C_{aromatic}$), 159.11 (CH = N) (Figure 2). Anal. calcd. for $C_{26}H_{36}N_4$; C: 77.22, H: 8.91, N: 13.86; Found; C: 77.05, H: 8.70, N: 13.64.

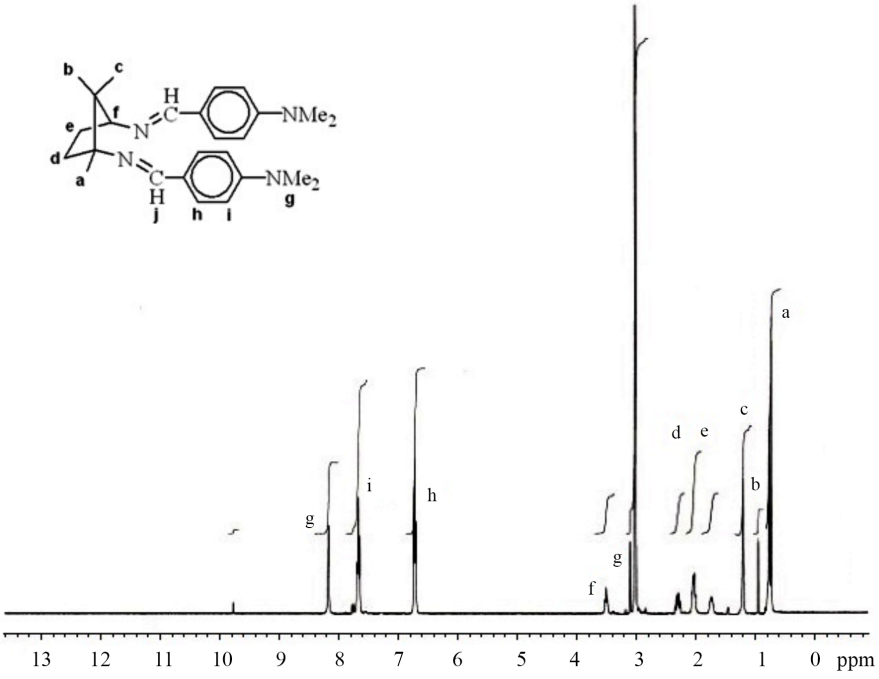


Figure 1. ^{1}H NMR spectrum of the monomer (**2**).

2.4. Polyimide synthesis

Polyimide synthesis was performed as follows: (1R,3S)-(+)-1,2,2-trimethyl-1,3-bis(p-dimethylamino benzyliden amino)-cyclopentane (2) (5 mmol) was dissolved in *N*-methyl-2-pyrrolidone (NMP) (15 mL) in a 50-mL Schlenk

tube equipped with a nitrogen line, overhead stirrer, a xylene-filled Dean–Stark trap, and a condenser. Pyromellitic dianhyride (PMDA) (1.09 g, 5 mmol) was added to the amine solution and stirred overnight to give a viscous solution. After being stirred for 3 h, the solution was heated to reflux at 145 °C for 15 h. During the polyimidization process, the water generated from the imidization was allowed to distill from the reaction mixture together with 1–2 mL of xylene. After being allowed to cool to ambient temperature, the solution was diluted with NMP and then slowly added to a vigorously stirred solution of 95% ethanol. The precipitated polymer was collected via filtration, washed with ethanol, and dried under reduced pressure at 150 °C. The polymer was isolated in 93% yield.

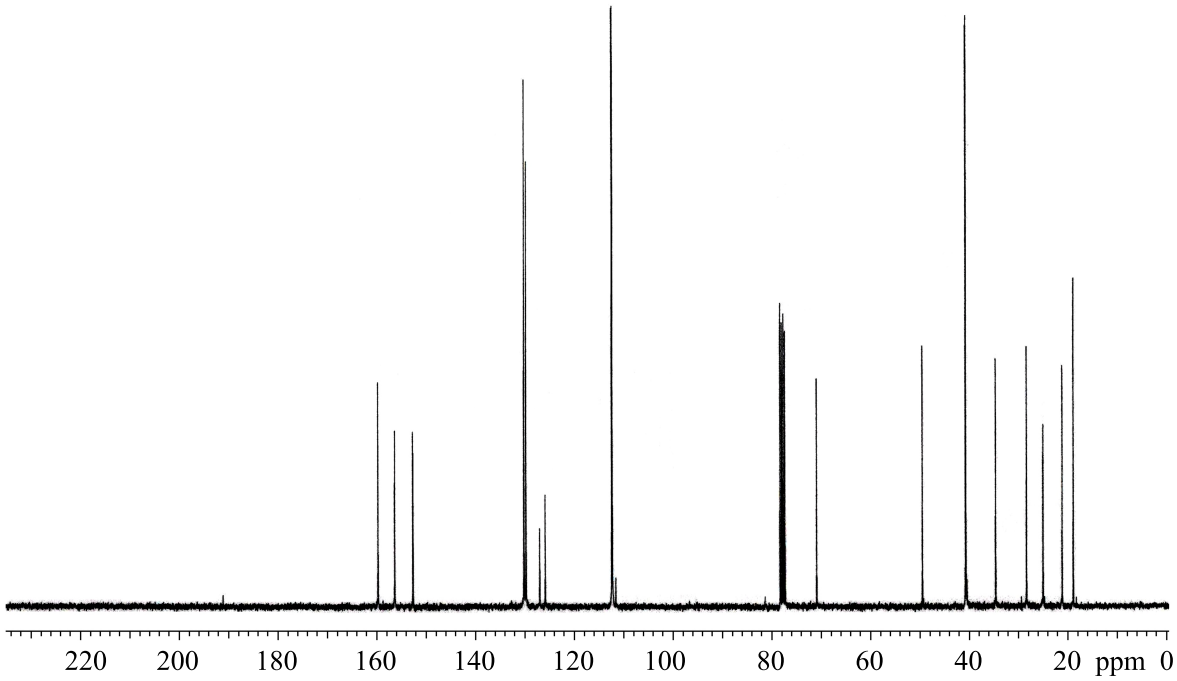


Figure 2. ^{13}C NMR spectrum of the monomer (**2**).

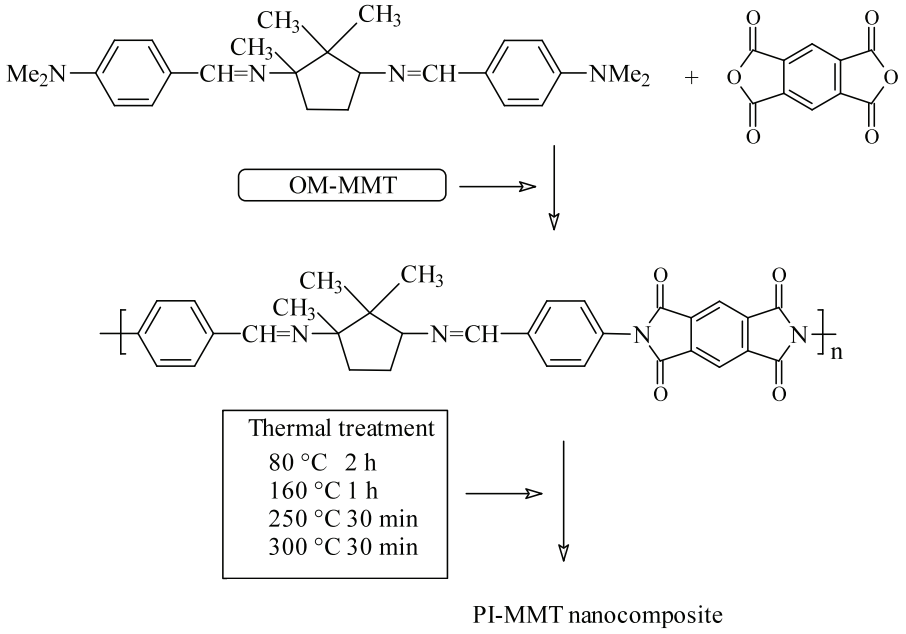
2.5. Synthesis of the PI–MMT nanocomposites

PI was synthesized by adding 0.025 mol of PMDA and 0.025 mol of (1R,3S)-(+)-1,2,2-trimethyl-1,3-bis(p-dimethylamino benzyliden amino)-cyclopentane (**2**) to NMP in a 100-mL 3-necked flask under nitrogen purge at 15 °C. The mixture was mechanically stirred for 20 h at room temperature and a viscous PI solution was obtained. PI–clay hybrids were prepared by blending OM-MMT suspension in NMP with PI solution. The total solid (PI–MMT) concentration was adjusted to 5 wt % by adding NMP. The mixtures were stirred for 5 h under nitrogen at room temperature to achieve complete dispersion of O-MMT in the PI, and were then cast on a carefully balanced slide glass, dried in a vacuum oven at 30 °C for 24 h, and cured with a series of thermal treatments to obtain yellow transparent PI films: 80 °C for 2 h; 160 °C for 1 h followed by 250 °C for 30 min and 300 °C for 30 min. The procedure for the preparation of PI–clay hybrids is summarized in Scheme 2.

3. Results and discussion

Polyimide–clay hybrid composite films were developed from the polyimide solution of (1R,3S)-(+)-1,2,2-trimethyl-1,3-bis(p-dimethylamino benzyliden amino)-cyclopentane with different weight percentages (1, 5, 10

wt %) of clay using *N*-methyl-2-pyrrolidone (NMP) as aprotic solvent using a combination by dissolving the polyimide and clay particles. We demonstrated the formation of composites with uniform particle dispersion. The microstructures and morphology of the as-obtained samples were studied by infrared spectra (IR), a scanning electron microscope equipped with an energy-dispersive X-ray spectrometer, and TGA.



Scheme 2. The preparation of the PI–MMT nanocomposites from solution of polyimide and with different weight percentages (1, 5, 10 wt %) of the organo-modified montmorillonite (OM-MMT).

3.1. Organo-modification of MMT

As previously mentioned, the organo-modification of MMT is an important step in the preparation of polymer-MMT nanocomposites and primary aliphatic amines such as 1-hexadecylamine and its quaternary ammonium salt were commonly used organic modifiers. In this study we used hexadecylpyridinium chloride. IR and XRD were used to verify that the organic modifiers designed by us have the same efficacy as the commonly used modifiers. Figure 3 shows the IR spectra of natural MMT, MMT, and OM-MMT. The absorption bands at 1038 and 1090 cm^{-1} were characteristic of Na-MMT (Figure 3). After the treatment, OM-MMT exhibited the characteristic bands of C–H stretching at 2914 and 2847 cm^{-1}.

The IR results only suggested that the treated MMT contained the organic modifiers; they could not support the conclusion that the molecules of organo-modifiers entered the galleries of MMT. Figure 4 shows the XRD patterns of natural MMT, MMT, and OM-MMT. The basal spacing of MMT was calculated from Bragg's equation. The interlayer spacing of MMT was obviously increased after the treatment from d = 1.24 nm for purified MMT to d = 2.90 nm for OM-MMT with hexadecylpyridinium chloride. This suggested that the organo-modifiers synthesized by us successfully intercalated between layers of MMT. More importantly, it has been widely accepted that the basal spacing of MMT treated by long-chain aliphatic amine is decided largely by chain length and long chain length leads to high d-values.

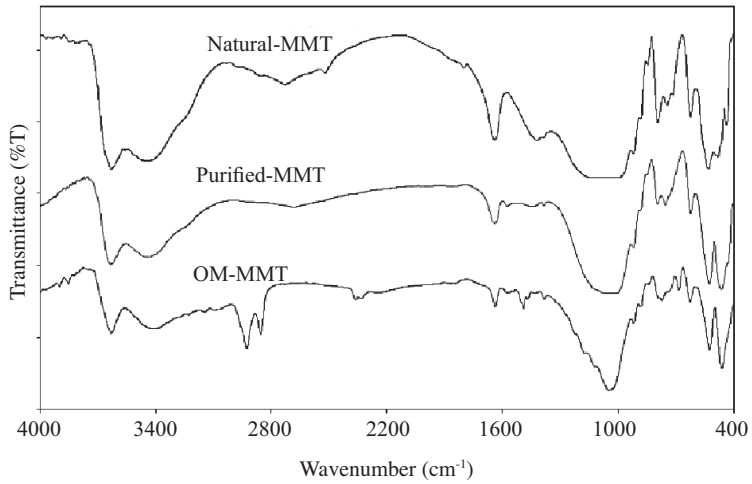


Figure 3. The IR spectra of natural MMT, MMT, and OM-MMT.

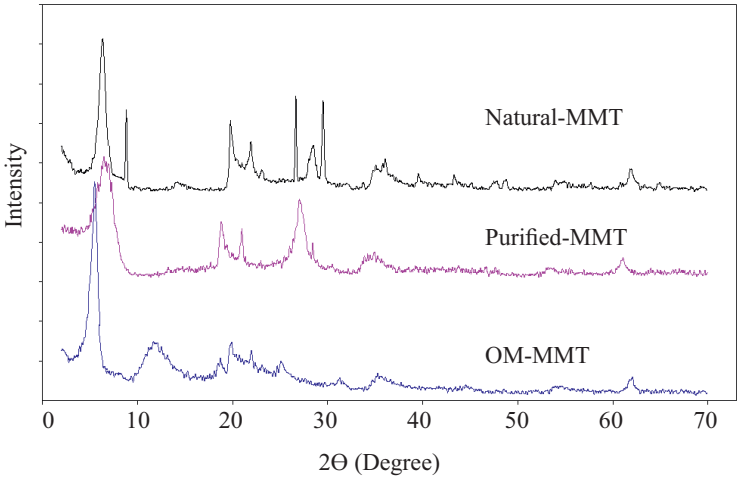


Figure 4. The XRD patterns of natural MMT, MMT, and OM-MMT.

3.2. Thermal stability of organo-modified MMT

Figure 5 shows the TGA curves of organo-modified MMT, illustrating 2- or 3-step degradation in the temperature range of 200–600 °C. This phenomenon was also observed and studied by Xie et al.[27] using DTA and MS. They proposed that the organics with a small molecular weight may be released first and those with a relatively high molecular weight may still exist between the interlayers until the temperature is high enough to lead to their further decomposition.[27] The initial thermal decomposition temperature (onset temperature) of OM-MMT was 252 °C. Natural MMT and MMT clearly showed higher initial thermal decomposition temperatures compared to OM-MMT.

The DTA curves of natural MMT, purified MMT, and organo-modified MMT are shown in Figure 6. We found that the DTA curves of the purified MMT do not vary significantly from that of natural MMT. However, OM-MMT shows 2 large thermal degradation peaks (between 225 °C and 425 °C) due to its organic groups.

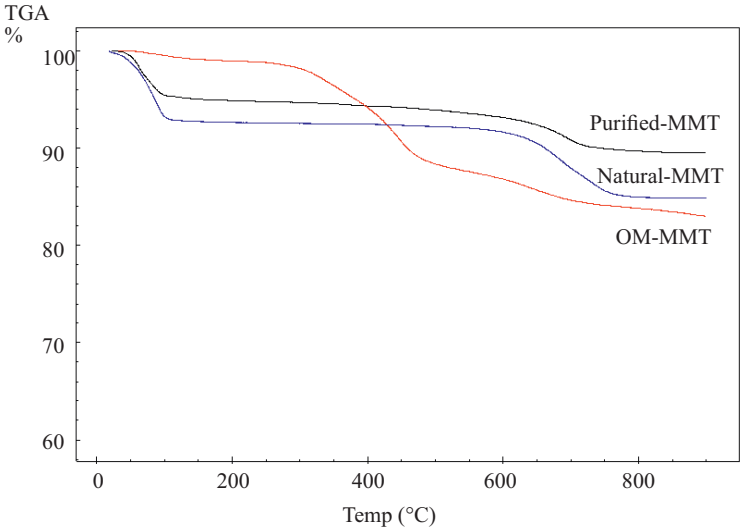


Figure 5. The TGA curves of natural MMT, MMT, and organo-modified MMT.

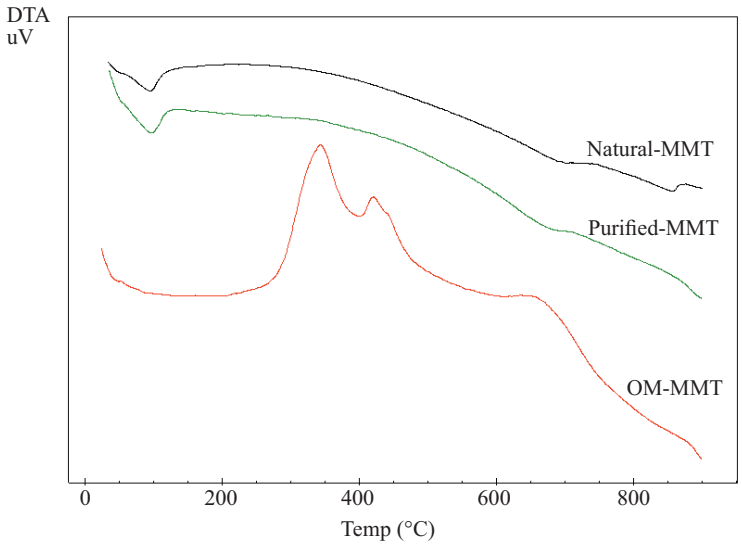


Figure 6. DTA curves of natural MMT, purified MMT, and organo-modified MMT.

3.3. FT-IR, XRD, and SEM characterization of PI–MMT nanocomposite films

The polymer and PI–clay nanocomposite were characterized by FT-IR spectra. The results are in agreement with the proposed structures. FT-IR spectra were collected in order to determine whether clay particles were incorporated into the polyimide matrix.

Figure 7 displays the FT-IR absorption spectra of pure PI and PI–MMT composites with various clay content and are recorded between 4000 and 650 cm^{-1}. The characteristic absorption peaks at 1780 cm^{-1} (C=O, asymmetric stretch), 1720 cm^{-1} (C=O, symmetric stretch), 730–725 cm^{-1} (C-N bending), and 1038 and 1090 cm^{-1} (Si-O-Si stretching) are clearly presented. The absorption bands at 1038 and 1090 cm^{-1} were characteristic of MMT. The absorption bands in IR results suggested that the PI–MMT contained clay. The intensity of absorption peaks increases with clay content.[15–19]

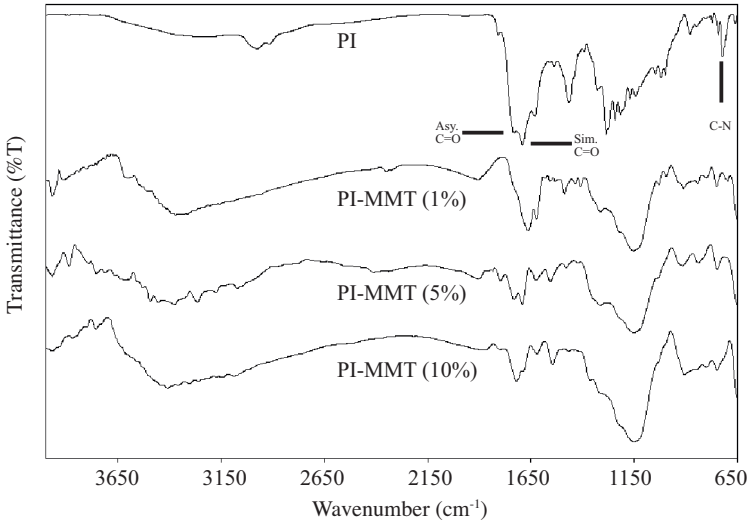


Figure 7. FT-IR spectra of the PI and PI–MMT composites.

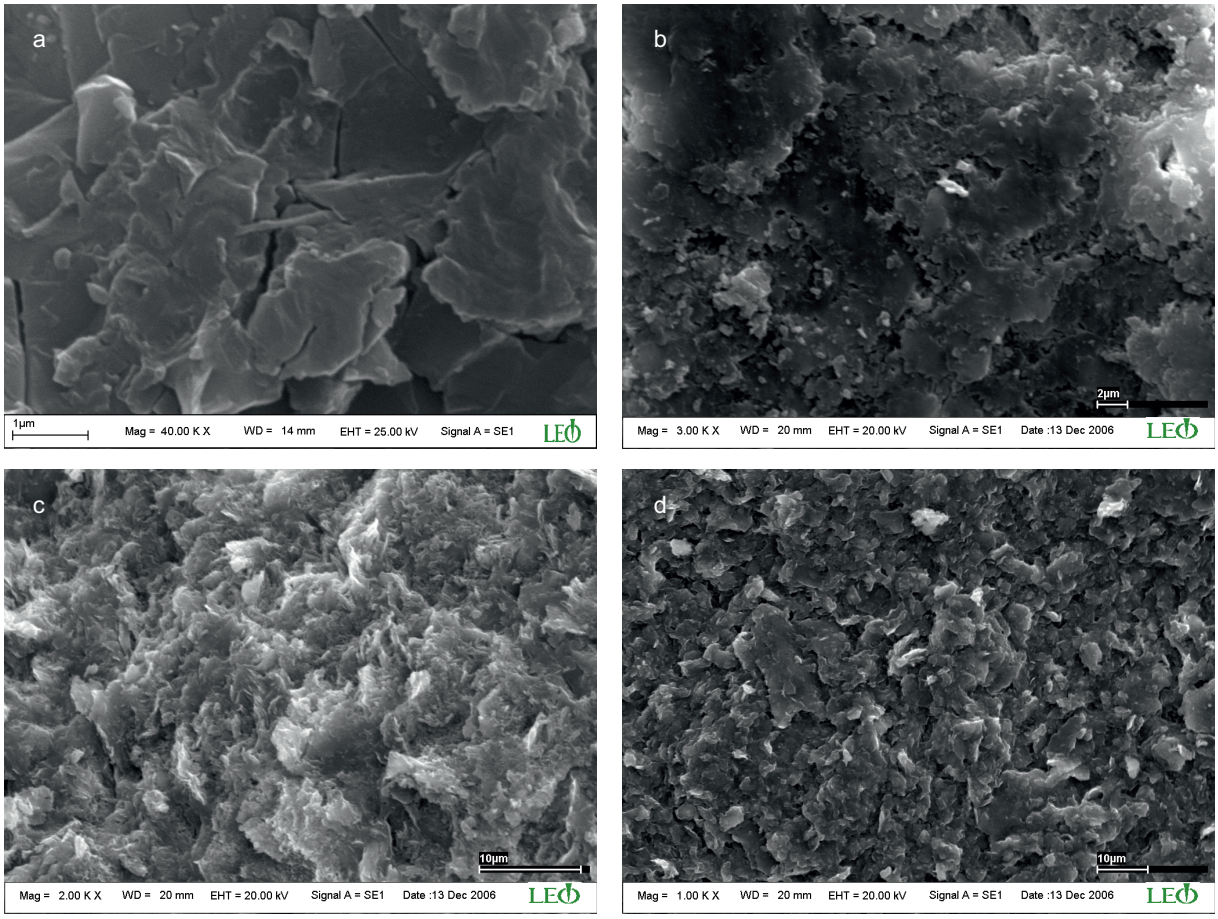


Figure 8. SEM image of pure PI (a) and PI–MMT composites with different loadings of clay in polymer (b) 1%, (c) 5%, (d) 10%.

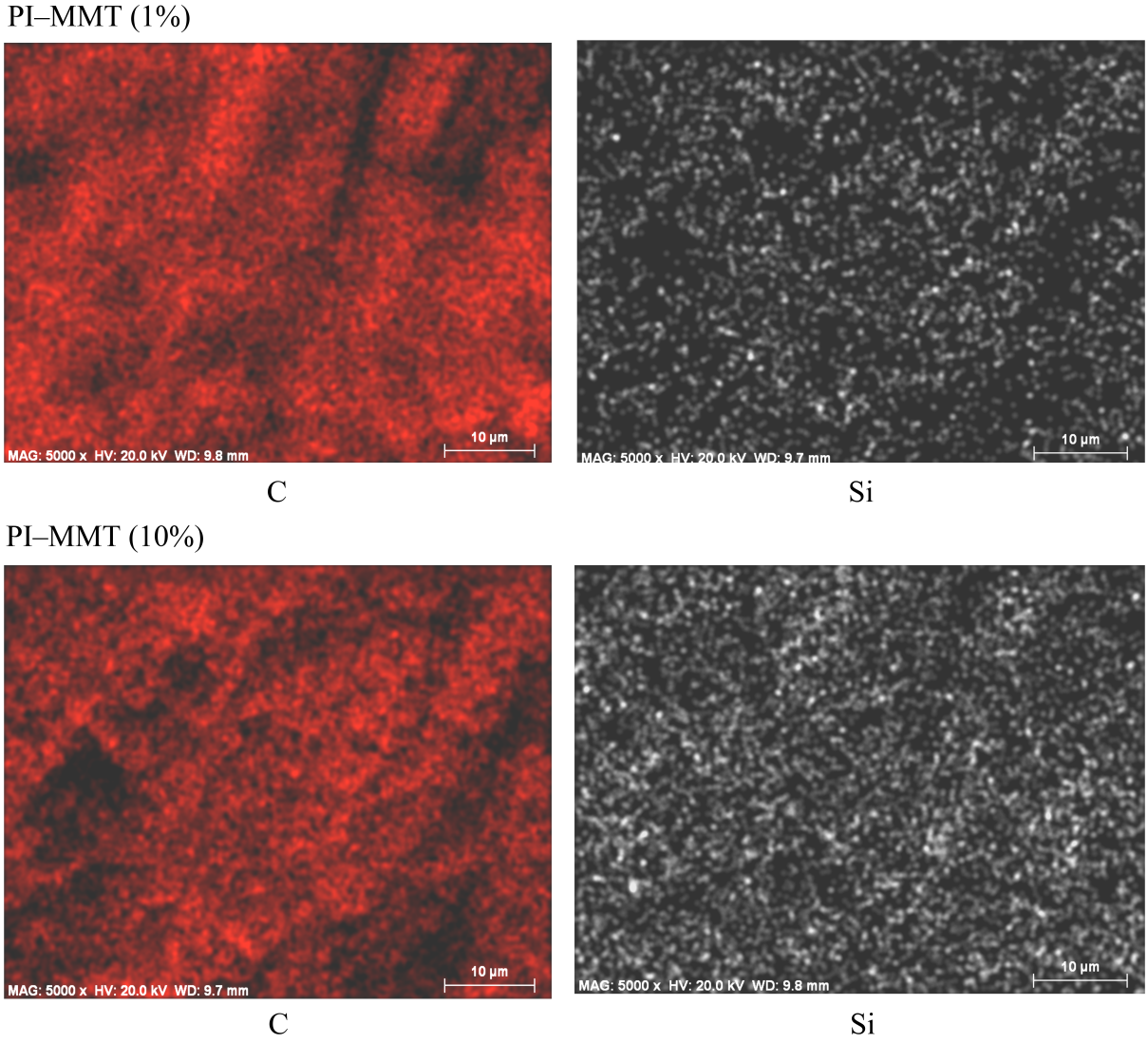


Figure 9. EDX mapping of the PI–MMT composites: PI–MMT (1%) and PI–MMT (10%).

Figure 8 shows the SEM photographs of the fracture surface of composite films. It can be clearly seen that the particles (clay) with a diameter of 400–700 nm are distributed uniformly in the polymer matrix for the hybrid films with 1 and 5 wt % of clay. In addition, we can also see that the clay particles are imbedded in polymer matrices, indicating that the clay has good compatibility and interfacial interaction with the polyimide matrix, which favors the improvement of the thermal and mechanical properties of hybrids. Energy-dispersive X-ray (EDX) analysis (Figure 9) demonstrated that clay seems to be dispersed randomly, although it does appear to form aggregates at increasing reinforcement loadings.

Figure 10 shows the XRD patterns of PI and the PI–MMT nanocomposite films with various MMT contents. There was no peak below 2h $= 10\theta$ for the pure polyamide film and the PI–clay nanocomposite film of 1 wt % clay. Although the clay content was low (1 wt %), XRD, which is a powerful and sensitive technique to detect the ordered structure by diffraction angle, revealed that the silicate layers in the PI–clay nanocomposite film of 1 wt % clay lost their ordered structure and were then separated. In other words, it could be supposed that the clay had been fully exfoliated and dispersed randomly in the polyimide matrix.[28,29] The diffraction

peak of MMT disappeared completely in the nanocomposites when the MMT content was below 5 wt %. This may indicate an exfoliated dispersion of MMT in PI. It is seen that the characteristic (001) diffraction peak of neat OM-MMT is located evidently around 2θ: 6.3° (d-spacing: 1.4 nm), whereas no discernible peak is observed for the PI–MMT-5% and PI–MMT-10% composites. This may indicate that the MMT layers with higher d-values were more favorable to the intercalation of PI molecules.

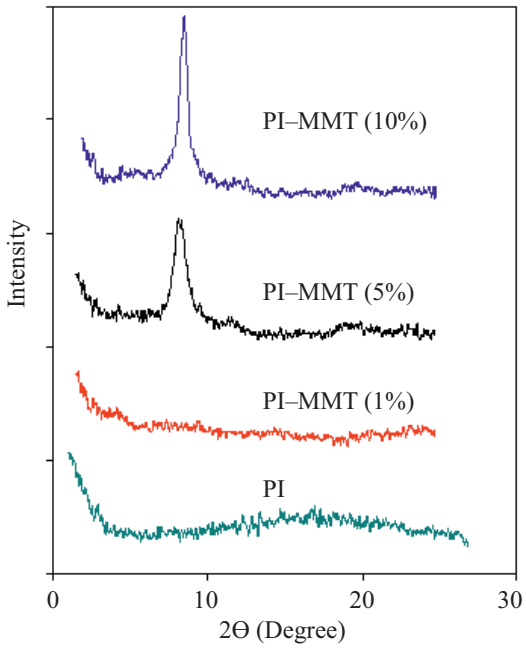


Figure 10. X-ray spectra of pure PI and PI–MMT composites with different loadings of clay in polymer (1% to 10%).

3.4. Thermal properties of PI–MMT nanocomposites

Figure 11 shows the TGA curves of PI–MMT nanocomposites with various MMT contents. The thermal stability of the nanocomposites was improved by the addition of OM-MMT. The on-set thermal decomposition

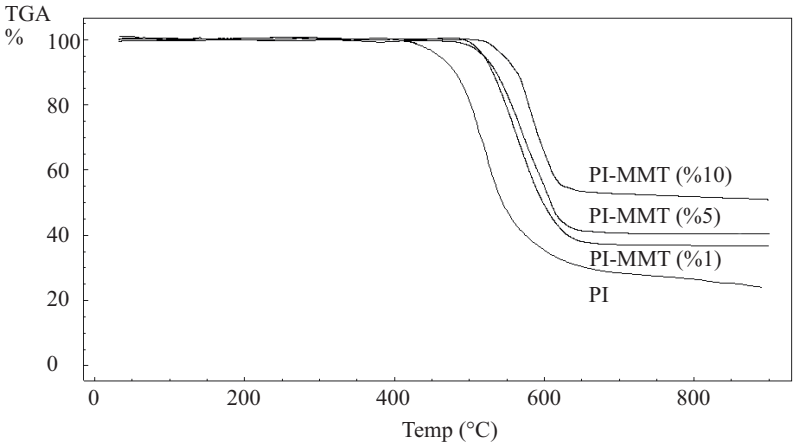


Figure 11. TGA of pure PI and PI–MMT composites with different loadings of clay in polymer (1% to 10%).

temperature accessed by TGA was increased from 433 °C for PI to 503 °C for PI–MMT nanocomposite containing 5 wt % MMT. MMT possessed high thermal stability and its layer structure exhibited a great barrier effect to hinder the evaporation of the small molecules generated in the thermal decomposition to limit the continuous decomposition of the PI matrix.

Figure 12 shows DSC traces of PI–MMT nanocomposites with various MMT contents. The Tg of the nanocomposites was slightly increased as the MMT content was increased. The Tg was increased from 270.1 °C for PI to 233.9 °C for the nanocomposite containing 1 wt % MMT and further to 276.7 °C for the nanocomposite containing 10 wt % MMT. This could be due to the strong interaction between MMT and PI, which limited the cooperative motions of the PI chain segments.

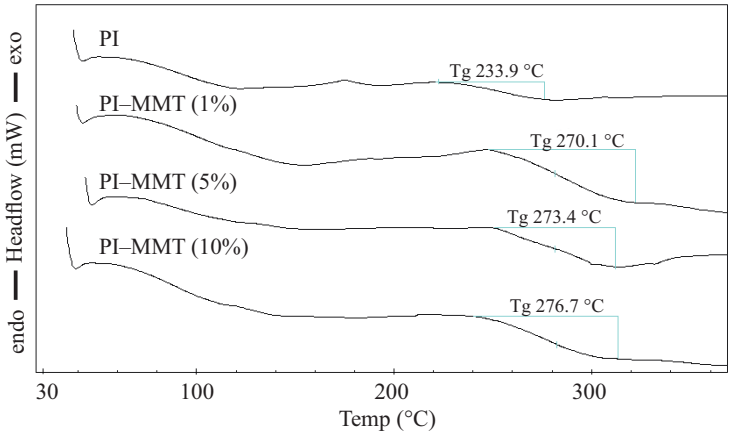


Figure 12. DSC of pure PI and PI–MMT composites with different loadings of clay in polymer (1% to 10%).

4. Conclusion

Thermally stable, rigid diamines were synthesized and used as monomers for polyimide and polyimide–MMT nanocomposites. The dispersion of organoclay in the polyimide matrix was achieved by applying mixing to the suspension of organoclay in polyimide solution. The X-ray spectroscopy confirmed the interaction between the polymer and silicate layers. The d-spacing of organoclay was found to be 1.71 nm compared to 0.97 nm of clay. The polyimide–clay nanocomposites formed an exfoliated structure with some disorder and their d-spacing was not significant. SEM results confirmed the dispersion of nanometer silicate layers in the polyimide matrix. The MMT content influenced the properties of PI–MMT nanocomposites significantly. The thermal stability of the PI–MMT nanocomposites was improved by the addition of OM-MMT. Moreover, the addition of clay showed higher Tg as compared with pure PI.

References

1. Schmidt, D.; Shah, D.; Giannelis. E. P. *Curr. Opin. Solid State Mater. Sci.* **2002**, *6*, 205–212.
2. Schmidt, G.; Malwitz, M. M. *Curr. Opin. Colloid Interface Sci.* **2003**, *8*, 103–108.
3. Sanchez, C.; Ribot, F.; Lebeau, B. *J. Mater. Chem.* **1999**, *9*, 35–44.
4. Morgan, A. B. *Polym. Adv. Technol.* **2006**, *17*, 206–217.
5. Tobushi, H.; Hayashi, S.; Hoshio, K.; Miwa, N. *Smart. Mater. Struct.* **2006**, *15*, 1033–1038.
6. Kawasumi, M.; Hasegawa, N.; Kato, M.; Okada, A. *Macromolecules* **1997**, *30*, 6333–6338.

7. Peng, Z. Q.; Chen, D. J. *J. Polym. Sci. B. Polym. Phys.* **2006**, *44*, 534–540.
8. Tian, M.; Qu, C. D.; Feng, Y. X. *J. Mater. Sci.* **2003**, *38*, 4917–4924.
9. Shen, L.; Lin, Y. J.; Du, Q. G.; Zhong, W.; Yang, Y. L. Polymer. **2005**, *46*, 5758–5766.
10. Lai, S. Q.; Yue L.; Li T. S.; Liu X. J.; Lv R. G. *Macromol. Mater. Eng.* **2005**, *290*, 195–201.
11. Utracki, L. A. J. *Nanosci. Nanotechnol.* **2008**, *8*, 1582–1596.
12. Carrado, K. A. *Appl. Clay. Sci.* **2000**, *17(1–2)*, 1–23.
13. Hussain, F.; Hojjati, M.; Okamoto, M.; Gorga, R. E. *J. Comp. Mater.* **2006**, *40*, 1511–1575.
14. Carastan, D. J.; Demarquette, N. R. *Int. Mater. Rev.* **2007**, *52*, 345–380.
15. Alexandre, M.; Dubois, P. *Mater. Sci. Eng.* **2000**, *R28*, 1–63.
16. Seçkin, T.; Köytepe, S.; Yiğit, M.; Çetinkaya, E. *Des. Monomers and Polym.* **2004**, *7*, 377–390.
17. Yiğit, M.; Seçkin, T.; Köytepe, S.; Çetinkaya, E. *Turk. J. Chem.* **2007**, *31*, 113–124.
18. Judenstein, P.; Sanchez, C. *J. Mater. Chem.* **1996**, *6*, 511–525.
19. Laine, R.; Sanchez, C.; Brinker, C. J.; Gianellis, E. *Hybrid Materials* Mater. Res. Soc., Pittsburgh, 1998.
20. Tsai, M. H.; Whang, W. T. *Polymer*, **2001**, *42*, 4197–4207.
21. Volksen, W.; Cotts, P.; Yoon, D. Y. *J. Polym. Sci. A-2.* **1987**, *25*, 2487–2495.
22. Köytepe, S.; Gök, Y.; Alıcı, B.; Seçkin, T.; Çetinkaya E. *Polym. Int.* **2004**, *53*, 688–697.
23. Seçkin, T.; Çetinkaya, E.; Köytepe, S.; Yigit, B. *Polym. Bull.* **2003**, *50*, 139-146.
24. Yano, K.; Usuki, A.; Okada, A. *J. Polym. Sci. Polym. Chem.* **1997**, *35*, 2289-2294.
25. Önal, M.; Sarıkaya, Y.; Alemdaroğlu, T.; Bozdoğan, İ. *Turk. J. Chem.,* **2003**, *27*, 683-693.
26. Serra, M. E. S.; Murtinho, D.; Goth, A.; Gonsalves, A. R.; Abreu, P. E.; Pais, A. C. *Chirality* **2009**, *22*, 425–431.
27. Xie, W.; Gao, Z.; Liu, K.; Pan, W. P.; Vaia, R.; Hunter, D.; Singh, A. *Thermochim. Acta.* **2001**, *367–368*, 339–350.
28. Meszaros, L; Czvikovszky, T. *Radiat. Phys. Chem.* **2007**, *76*, 1329–1332.
29. Mohanty, S.; Nayak, S. K. *Polym. Compos.* **2007**, *28*, 153–162.